

Supporting information

Tailoring hydroxyl groups of organic phenazine anode for high-performance and stable alkaline batteries

Huilin Cui^{1,2}, Dechao Zhang^{1,2}, Zhuoxi Wu¹, Jiaxiong Zhu¹, Pei Li^{1,2}, Chuan Li¹, Yue Hou^{1,2}, Rong Zhang^{1,2}, Xiaoqi Wang³, Xu Jin³, Shengchi Bai³, Chunyi Zhi^{1,2,4*}

¹ Department of Materials Science and Engineering, City University of Hong Kong, 83 Tat Chee Avenue, Kowloon, Hong Kong 999077, China.

² Hong Kong Center for Cerebro-Cardiovascular Health Engineering (COCHE), Shatin, NT, HKSAR, China.

³ Research Institute of Petroleum Exploration & Development (RIPED), PetroChina Research Center of New Energy, No. 20 Xueyuan Road Haidian District, Beijing, 100083, P. R. China

⁴ Hong Kong Institute for Clean Energy, City University of Hong Kong, Kowloon 999077, Hong Kong.

Corresponding E-mail: cy.zhi@cityu.edu.hk

Experimental section

Materials

All chemicals were purchased from commercial suppliers and used without any further purification, including phenazine (PZ, Aldrich), benzoquinone (Aldrich), 1,2-phenylenediamine (Aldrich) and 2,5-dihydroxy-1,4-benzoquinone (Aldrich), PTFE (Macklin), isopropyl alcohol (Macklin), potassium hydroxide (KOH, Aldrich), Lithium hydroxide (LiOH, Macklin), ketjenblack (KB, ECP-600JD, Lion Corporation), isopropanol alcohol (Aldrich), Pt/C (20 wt.% in Pt, Macklin), (Methyl sulfoxide)- d_6 (DMSO- d_6 , Aldrich), Nafion D-520 dispersion (5% w/w in water and 1-propanol, Alfa Aesar) and graphite oxide aqueous dispersion (GO, 10 mg/g, GaoxiTech). Carboxymethyl Cellulose Sodium (CMC, Aldrich) Phenazine derivatives of 2-hydroxyphenazine (PZ-OH) and 1,2-dihydroxyphenazine (PZ-2OH) were prepared according to the following Synthesis Method section described steps.

Electrochemical Measurements

The CR2032 coin-type cells were assembled in an air atmosphere for the electrochemical measurements of phenazine derivatives. The anodes were prepared by compressing the mixture of the phenazine derivatives powder, KB, and PTFE binder (mass ratio: 6: 2.5: 1.5) and a certain amount of isopropyl alcohol solvent on the nickel foam, after drying at 60 °C overnight under vacuum, the anode with a mass loading of 1-1.5 mg cm⁻² was obtained. 200 μL aqueous electrolyte with 6 M KOH and 1 M LiOH was employed as the electrolyte. For the phenazine derivatives || Ni (OH)₂ battery, an excess amount of Ni (OH)₂ was used as the cathode, and the Ni (OH)₂ electrode was obtained from the commercial nickel–metal hydride (Ni–MH) battery that can eliminate the impact of the cathode material on the electrochemical performance of the full cell. To control the n/p ratio, the Ni (OH)₂ electrodes were prepared by mixing the Ni (OH)₂ powder, CMC, and PTFE binder (mass ratio: 100: 0.5: 0.5) into deionized water and coated it on the foamed nickel current collector after drying it at 60 °C overnight finally. For the organic || Air battery, the Pt/C was used as the cathode, which was prepared as follows: 5 mg of Pt/C blended with 50 μL Nafion solution (5 wt% Nafion in the solution of isopropanol: water = 1:1 vol.) and

sonicated for 30 minutes, the obtained slurry was cast onto a clean carbon cloth and dried at 80°C for 12 h in a vacuum oven. For the full battery assembly, hydrophilic PP complex sulfonated cellulose membrane as the separator. Besides, a free-standing graphene oxide (GO) film was inserted between the anode and the separator to inhibit the dissolution of anode materials, which was prepared by a simple filtration method. Firstly, 1 g GO aqueous was dispersed into 40 mL ethanol and ultrasonic treatment for 60 min. Then, the obtained suspension solution was filtered and dried at 70 °C for 24 h. Finally, the free-standing GO film (mass: 0.6 mg cm⁻²) was obtained after peeling it off from the filter paper. In three electrode system, the phenazine derivative, Pt metal, and Hg/HgO were used as cathodes, counter electrodes, and reference electrodes, respectively. While, the rate performance of phenazine derivative electrode was tested by assembling phenazine derivative and active carbon forming two electrodes to inhibited the partial dissolution of phenazine derivatives. Cyclic voltammetry (CV) and Electrochemical Impedance Spectroscopy (EIS) curves were carried out on an electrochemical workstation (CHI 760E). The galvanostatic discharge/charge tests, rate capability, and cycle performance were measured on battery test systems (LAND CT2001A). The cyclic performance, electrochemical properties of batteries were characterized by the LAND CT2001A device and electrochemical workstation CHI 760D at 25 °C. The above electrochemical properties were measured at 25 °C. The low-temperature performance of PZ-2OH || Ni (OH)₂ battery was tested in a cryogenic box (-30~20 °C). All current densities, specific capacities, and energy densities in this work were calculated based on the mass of phenazine derivatives anode material. All the batteries were activated in the initial three cycles at the current density of 0.2 A g⁻¹. For each electrochemical test, at least three-coin cells were assembled for test.

Material Characterizations

The proton nuclear magnetic resonance (1H NMR) was collected using Nuclear Magnetic Resonance 300 (NMR 300). The Fourier-Transform Infrared Spectroscopy (FT-IR) was obtained on a PerkinElmer Spectrum II spectrometer to characterize the changes of the specific chemical groups. X-ray diffractometer equipment (XRD;

Bruker, D2 Avance) was used to record the XRD pattern. The morphology and microstructure were observed by scanning electron microscope (SEM; SU4800, Hitachi). Thermogravimetric- Differential scanning calorimetry synchronous thermal analyzer (TG-DSC) was carried out on Mettler TGA/DSC3+ to obtain the thermodynamic stability of materials, and the heating rate is 5 °C min⁻¹ from room temperature to 500 °C under N₂. X-ray photoelectron spectroscopy (XPS; ESCALAB 250) was performed to analyze surface compositions. Raman spectroscopy was conducted on a WITec alpha300 access equipped with a laser of 532 nm to record the changes in chemical bonds during charge/discharge reactions. Specific Surface Area and Porosimetry Analyzer (BET; Micromeritics ASAP 2460/2020) was performed to analyze surface area and pore structures. The Raman spectrum was carried out using WITec alpha300 access with a laser of 532 nm wavelength. A coin cell with a quartz window on the positive shell was used for in situ Raman spectroscopy analysis. The ex-suit FTIR and XPS were performed after washing the charging/discharging electrode with different potential.

Theoretical Calculations

All DFT simulations were performed by the Gaussian 16 software package. The structures and the energy levels of the highest occupied molecular orbital (HOMO) / lowest unoccupied molecular orbital (LUMO) of phenazine derivatives were fully optimized at B3LYP/6-31+G (d, p) level. Molecular electrostatic potential (ESP) results were performed with Multiwfn 3.3.9 programs¹ and the visualization of ESP plots was carried out by Visual Molecule Dynamics (VMD) software. The electron affinity is defined by the change of the free energy between the neutral system to the negatively charged system.

To calculate the theoretical reduction potential for these phenazine derivatives, we calculated the Gibbs free energy for all the compounds involved in the reduction reaction. The geometric optimizations were performed for the neutral and reduced forms of the phenazine derivatives in the solvent phase using the B3LYP functional in combination with the 6-31+G(d, p) basis set. All DFT calculations were performed with the Gaussian 16 software package.

The reduction potentials of the phenazine derivatives (PZD) were calculated using the reaction: $[PZ]^{+} + [PZD] \rightarrow [PZ] + [PZD]^{-}$, relative to the corresponding values for the reference species, the parent phenazine (PZ). The following equation was used:

$$E_{red} = \frac{\Delta G_{rea}}{nF} + E_{(ref)} \quad (1)$$

where $E_{(ref)}$ is the experimentally measured reduction potential of the phenazine, ΔG_{rea} is the free energy change of the reaction in the solution, F is the Faraday constant and n is the number of electrons involved in the reduction process. This approximation has been used successfully previously to calculate the reduction potentials of organic molecules in both aqueous and non-aqueous solvents.

Calculation of the energy density and power density

The energy density E (W h kg⁻¹) and power density P (W kg⁻¹) values of the battery were calculated as follows:

$$E = \frac{\int IV(t)dt}{3.6m} \quad (1)$$

$$P = \frac{3600 E}{t} \quad (2)$$

Where the I is the applied current (A), V is the potential of device (V), t is the discharge time (s), and m is the weight of electrode (g).

Calculation of the capacity decay rate per cycle:

The following equation was used to calculate the capacity decay rate per cycle:

$$\text{The capacity decay rate per cycle} = \frac{C_a - C_i}{C_i} \cdot \frac{1}{n} \quad (3)$$

Where C_a , C_i and n presents the capacity of after cycle, the capacity of initial and cycle numbers, respectively.

Calculation of the ion diffusion coefficient (D) from GITT Tests

The D was measured by using Galvanostatic Intermittent Titration Technique (GITT) and calculated based on the following equation:

$$D = \frac{4}{\pi\tau} \left(\frac{m}{\rho S} \right)^2 \left(\frac{\Delta E_s}{\Delta E_t} \right)^2$$

Where t and τ represent the duration of current pulse (s) and relaxation time (s), respectively. m , ρ and S is the mass (g), density and electrode area (cm^2) of the active material. ΔE_s and ΔE_t are the steady-state voltage change (V) by the current pulse and voltage change (V) during the constant current pulse (eliminating the voltage changes after relaxation time).

Calculation of the activation energy (E_a) from EIS Tests

The E_a was calculated according to the EIS spectra at different temperature, which can be calculated by the following equation²:

$$1/R_{ct} = A_0 e^{-E_a/RT} \quad (4)$$

Where R_{ct} , R and T presents the charge transfer resistance (Ω), gas constant ($8.314 \text{ J mol}^{-1} \text{ K}^{-1}$), and the testing temperature (298 K), respectively.

Calculation of the Capacitive Contribution

The ion and electron transport kinetics and the capacitive contribution were calculated according to the following equation³:

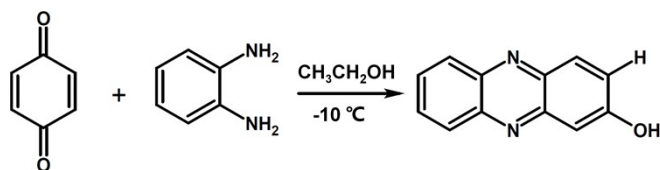
$$i = k v^b \quad (5)$$

where k and b are constants. The above equation can be rearranged as follow:

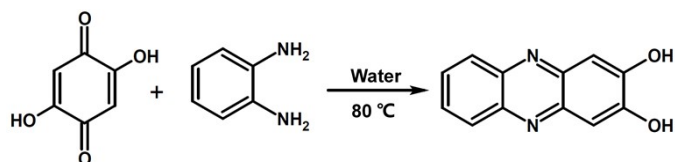
$$\log(i) = \log(k) + b * \log(v) \quad (6)$$

By linear plotting $\log(i)$ versus $\log(v)$, the value of b can be obtained.

Synthesis Method



Synthesis of 2-hydroxyphenazine (PZ-OH): Firstly, the benzoquinone (1.08 g, 10 mmol) was added into an anhydrous alcohol solution (100 mL), forming solution A. Then, 1,2-phenylenediamine (1.08 g, 10 mmol) was dropped into solution A at $-10\text{ }^{\circ}\text{C}$ and continuously stirred for 2 h. Finally, the obtained mixture was concentrated to 10 mL at reduced pressure, and 50 mL of deionized water was poured into the concentrated mixture.⁴ The resulting suspension was filtered and washed with deionized water until the filtrate was colorless. The yield of PZ-OH was about 70%.



Synthesis of 1,2-dihydroxyphenazine (PZ-2OH): Firstly, the 2,5-dihydroxy-1,4-benzoquinone (0.71 g, 0.51 mmol) and 130 mL DI water were mixed in a round bottomed flask under a nitrogen atmosphere, forming solution A at $80\text{ }^{\circ}\text{C}$. Then, 1,2-phenylenediamine (0.5 g, 0.46 mmol) was dropped into solution A and continuously stirred for 7 h. Finally, the mixture was naturally cooled to room temperature and stirred overnight.⁵ The resulting suspension was filtered and washed with deionized water until the filtrate was colorless. The yield of PZ-OH was about 80%.

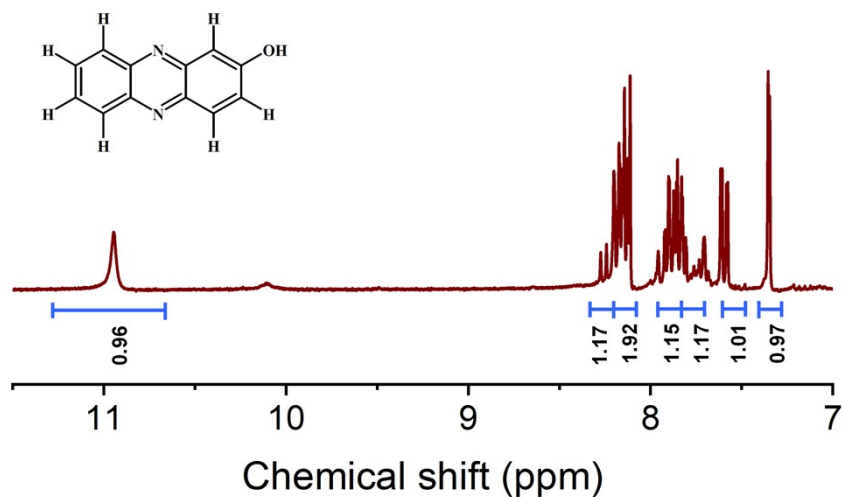


Figure S1. ^1H NMR spectrum of PZ-OH (300 MHz, $\text{DMSO-}d_6$) δ 10.95 (s, 1H), 8.19 (dd, $J = 8.7, 1.5$ Hz, 1H), 8.13 (dd, 1H), 7.90 (ddd, $J = 8.6, 6.6, 1.7$ Hz, 1H), 7.83 (ddd, $J = 8.2, 6.6, 1.6$ Hz, 1H), 7.60 (dd, $J = 9.4, 2.6$ Hz, 1H), 7.35 (d, $J = 2.6$ Hz, 1H).

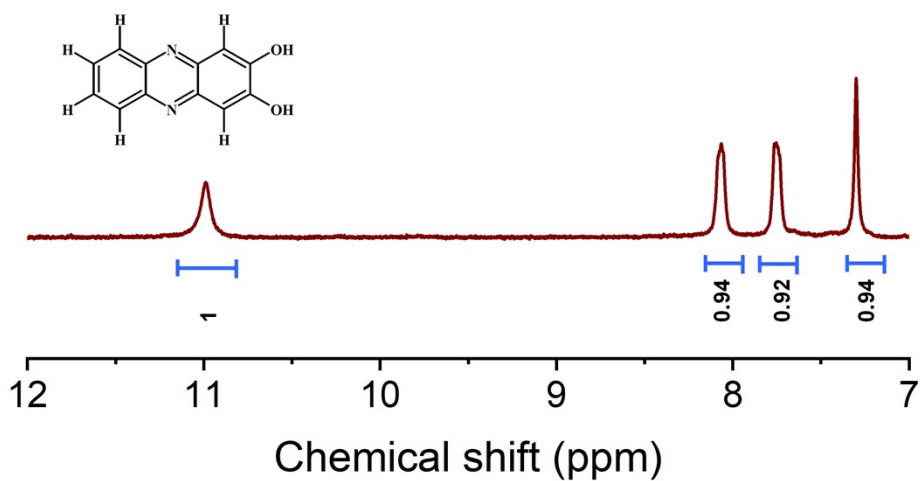


Figure S2. ^1H NMR of PZ-2OH (300 MHz, $\text{DMSO-}d_6$) δ 10.99 (s, 2H), 8.07 (s, 2H), 7.74 (s, 2H), 7.30 (s, 2H).

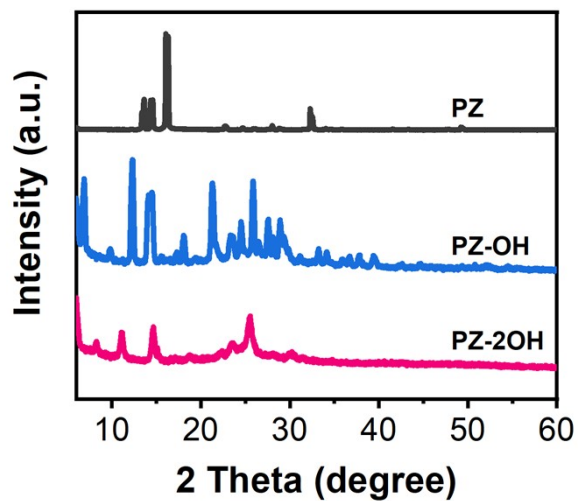


Figure S3. XRD patterns of the synthesized PZ, PZ-OH, PZ-2OH.

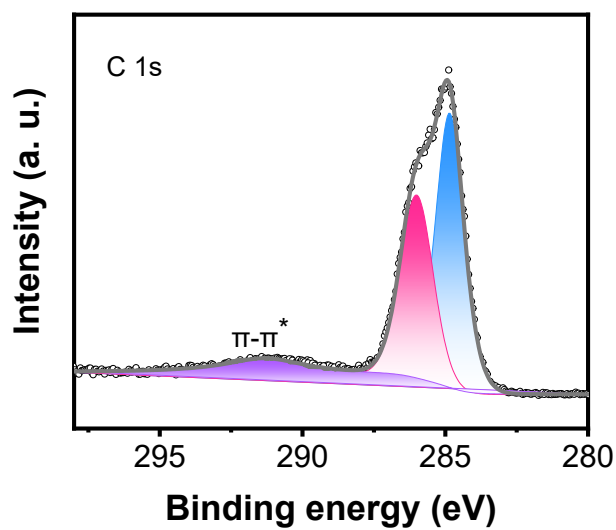


Figure S4. The high-resolution C 1s XPS of PZ-2OH.

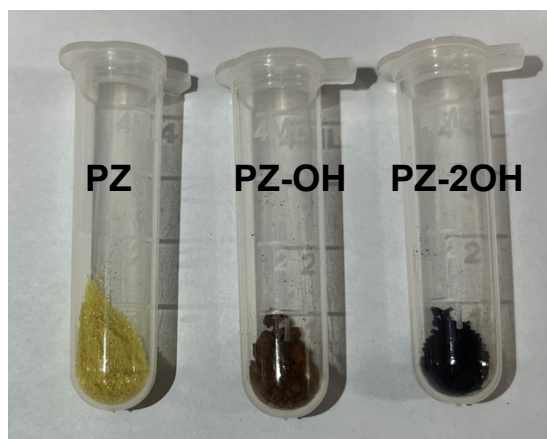


Figure S5. Optical photographs of the as-synthesized PZ, PZ-OH, PZ-2OH.

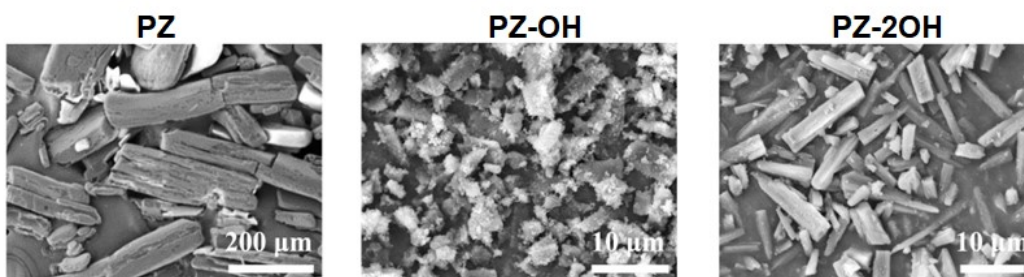


Figure S6. Scanning electron microscope (SEM) images of the as-synthesized PZ, PZ-OH, PZ-2OH.

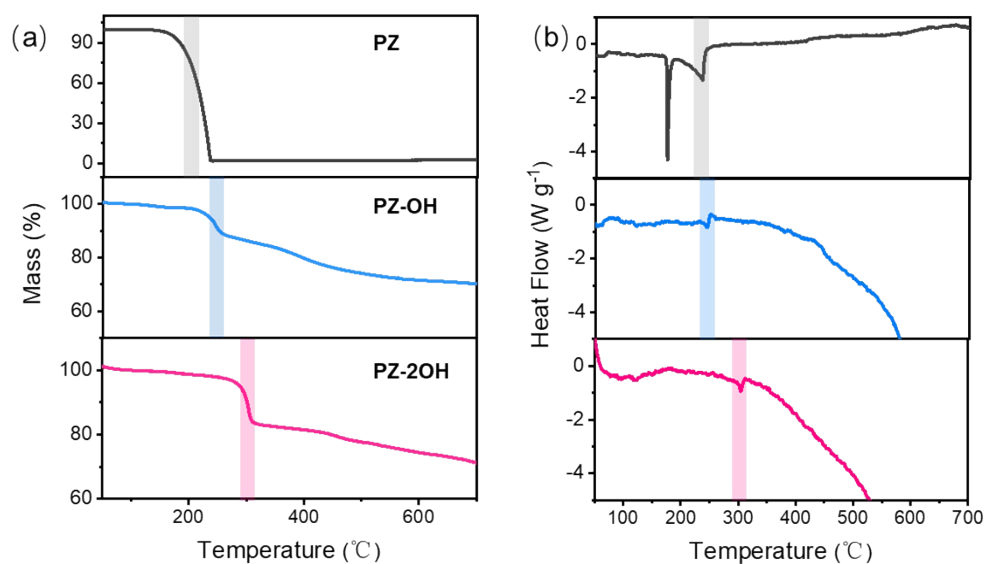


Figure S7. (a) TGA curves and (b) DSC curves of PZ, PZ-OH and PZ-2OH under an N_2 atmosphere.

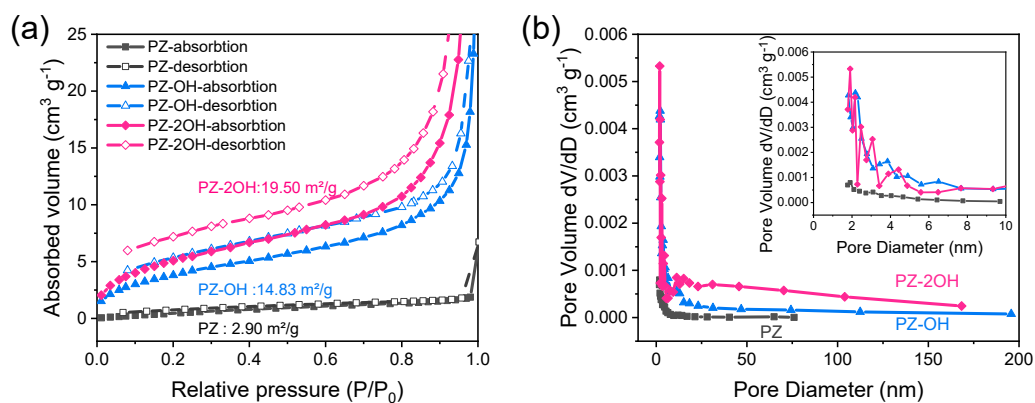


Figure S8. (a) Nitrogen adsorption-desorption isotherms and (b) pore size distribution

of phenazine derivative.

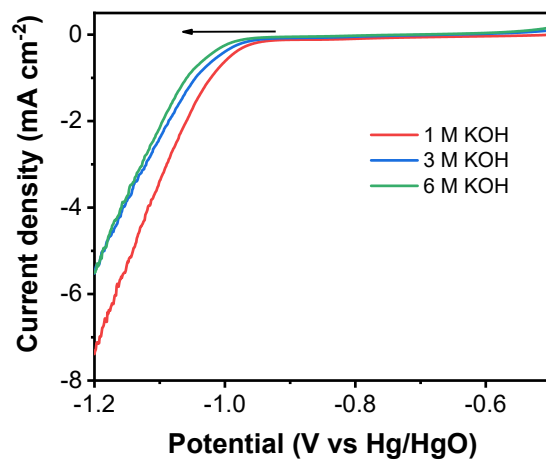


Figure S9. The linear sweep voltammetry (LSV) of carbon cloth in different concentrations KOH electrolyte.

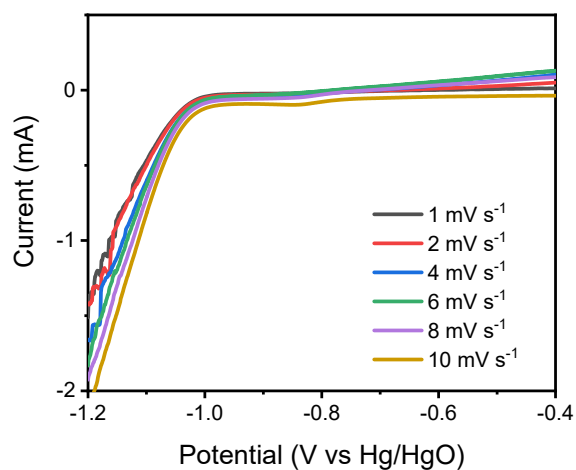


Figure S10. The linear sweep voltammetry (LSV) of carbon cloth in 6 M KOH electrolyte at different scan rate.

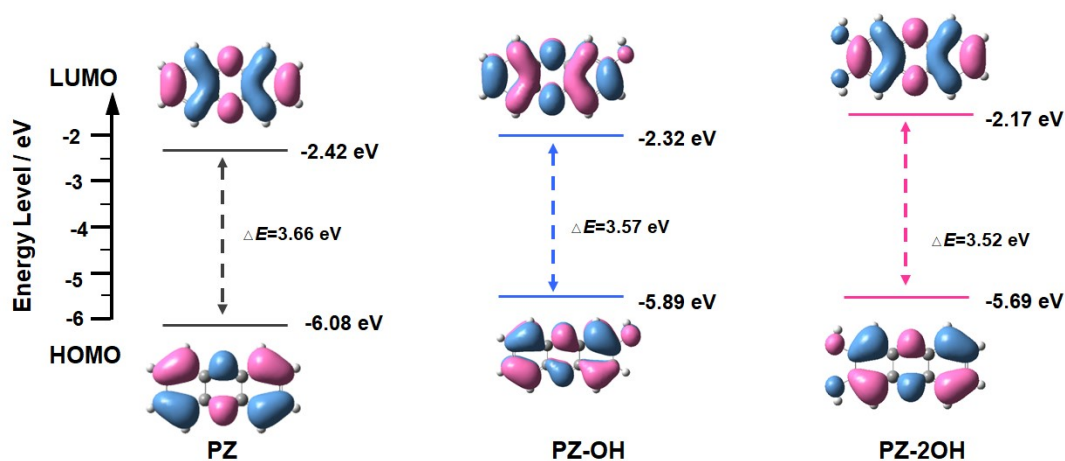


Figure S11. Optimized structure and calculated LUMO and HOMO energy levels of PZ, PZ-OH and PZ-2OH.

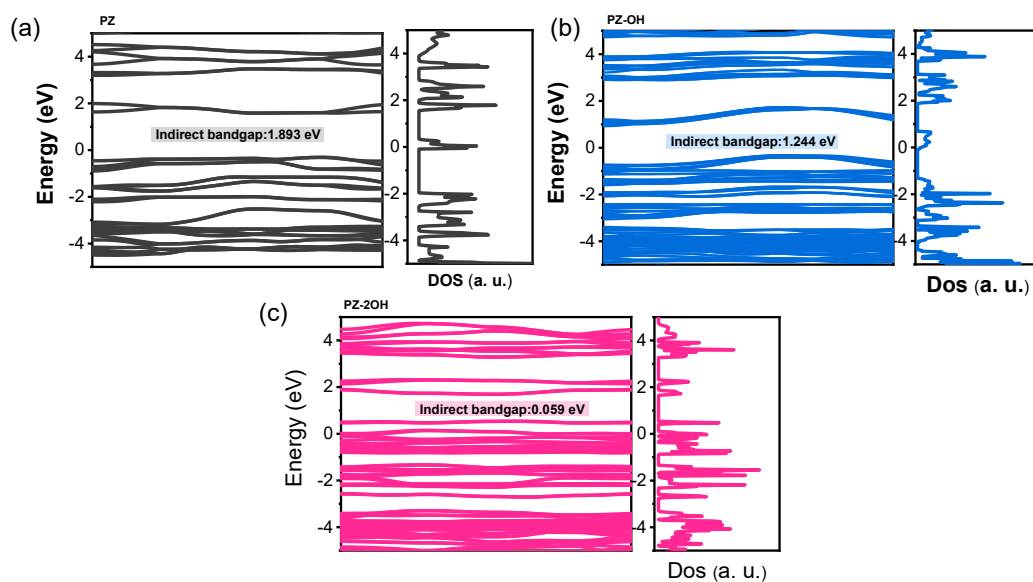


Figure S12. The calculated band structures of PZ (a), PZ-OH (b) and PZ-2OH (c).

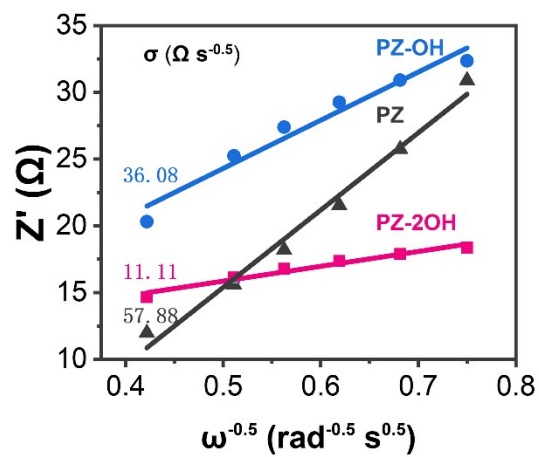


Figure S13. The relationship between the real part of the impedance and $\omega^{1/2}$.

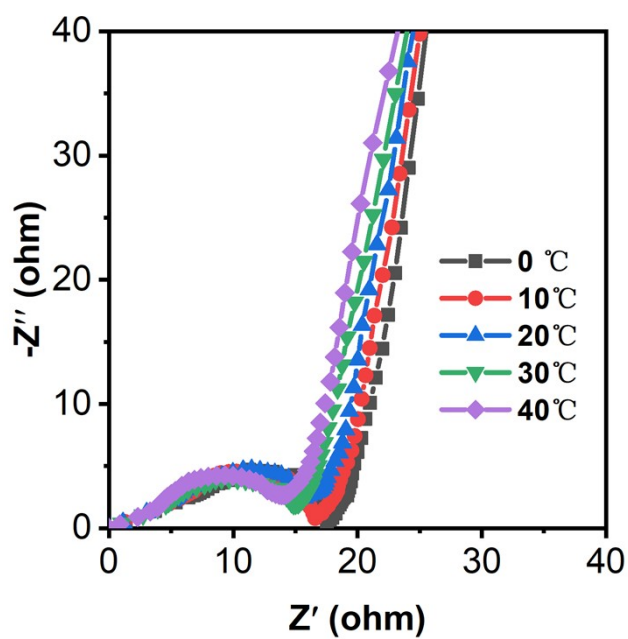


Figure S14. Nyquist plots at various temperatures of PZ-2OH.

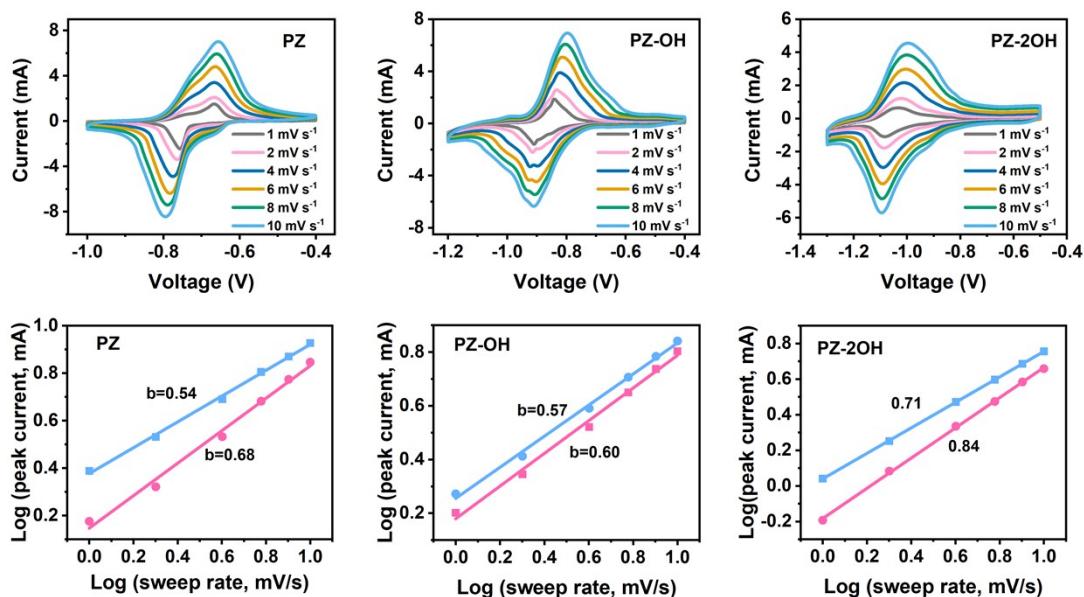


Figure S15. CV curves at a scan rate of 1, 2, 4, 6, 8 and 10 mV s^{-1} and the corresponding $\log i_{\text{peak}}$ versus $\log v$ of PZ, PZ-OH and PZ-2OH. (blue line represent the reduction peak and the red line represent the oxidation peak).

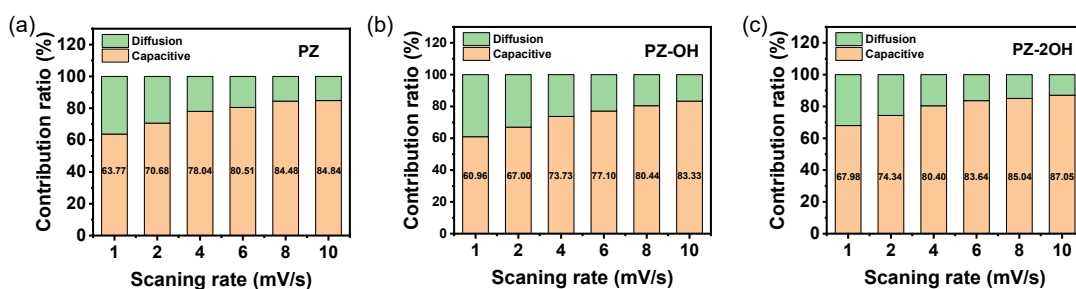


Figure S16. The capacitive contributions of PZ, PZ-OH and PZ-2OH at different scan rates.

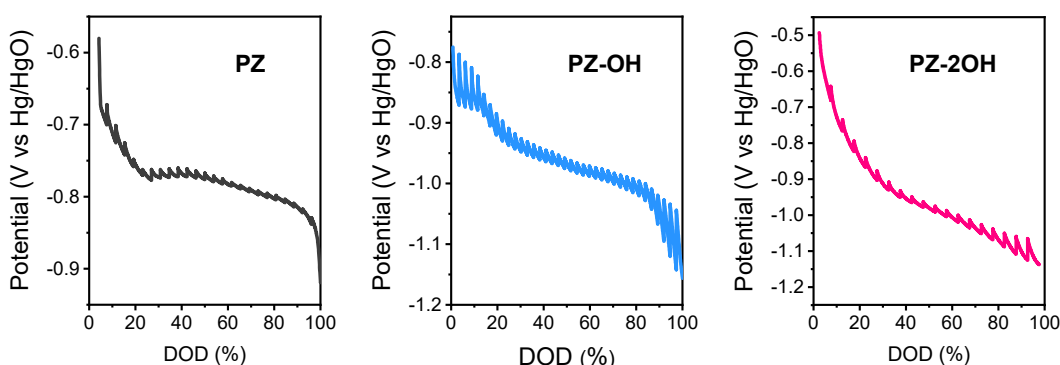


Figure S17. GITT curves for phenazine derivative.

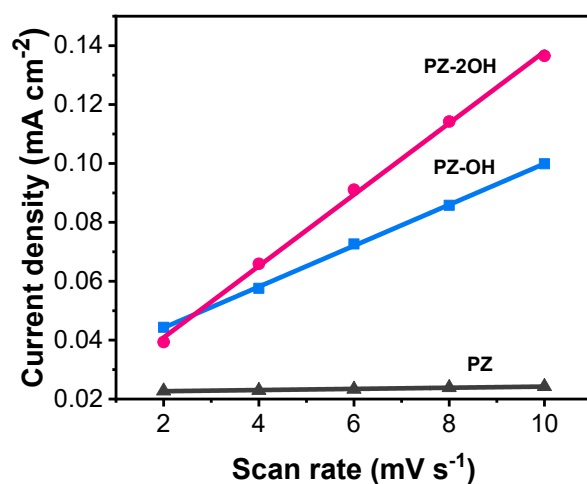


Figure S18. The capacitive current density at the potential of 0.9-1 V (non faradic region) as a function of scan rate for Phenazine derivatives symmetric cell.

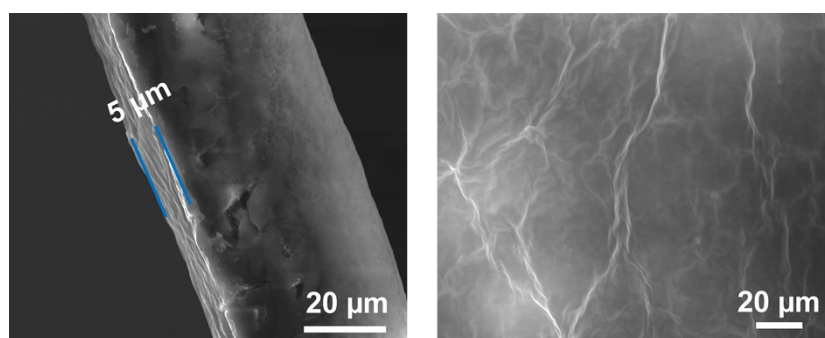


Figure S19. SEM images of GO membranes. (a) Cross-section morphology and (b) surface morphology of GO membrane. The thickness of the film is about 5 μm and the weight is 0.67 mg cm^{-2} .

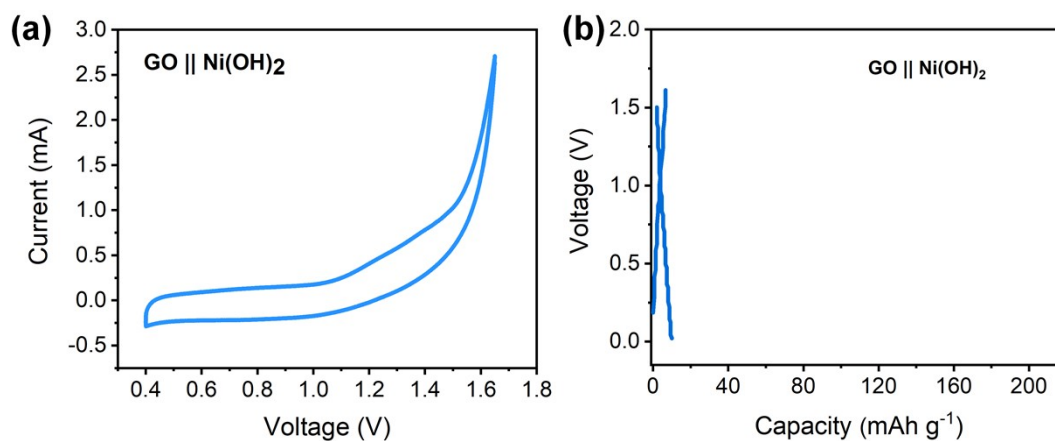


Figure S20. Electrochemical performance of GO || Ni(OH)₂ battery. (a) CV profile at

0.5 V s⁻¹. (b) GCD profile at 0.2 A g⁻¹, which confirmed the capacity contribution of the GO membrane was negligible.

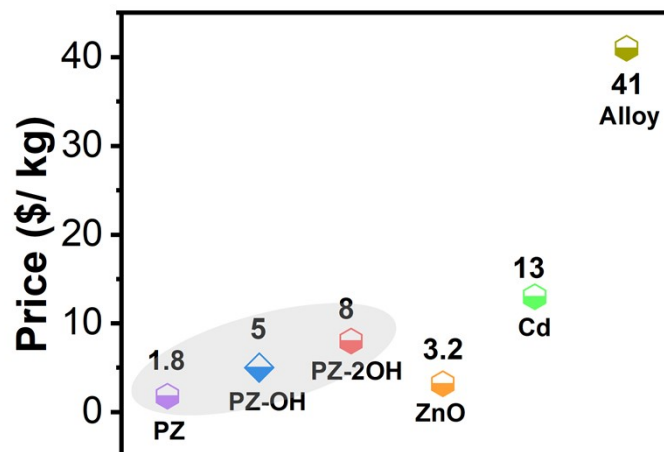


Figure S21. The price comparison of the prepared phenazine derivatives with other anode materials for alkaline nickel-based batteries.

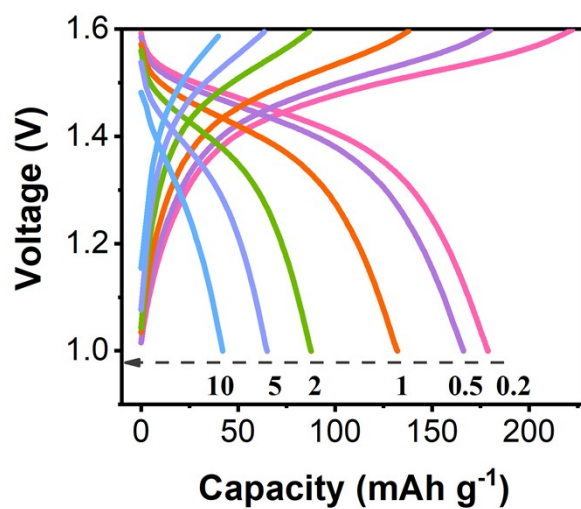


Figure S22. GCD curves of PZ-2OH || Ni(OH)₂ at the current density of 0.2 A g⁻¹, 0.5 A g⁻¹, 1 A g⁻¹, 2 A g⁻¹, 5 A g⁻¹.and 10 A g⁻¹.

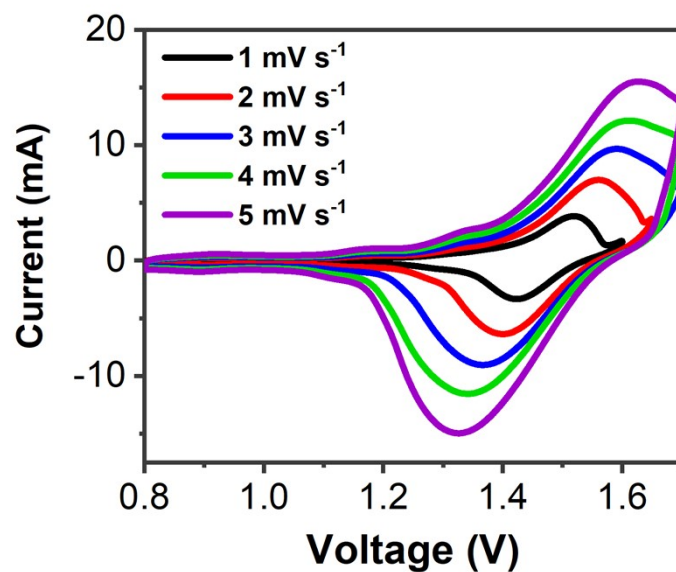


Figure S23. CV curve of PZ-2OH || Ni(OH)₂ full cell at different scan rates.

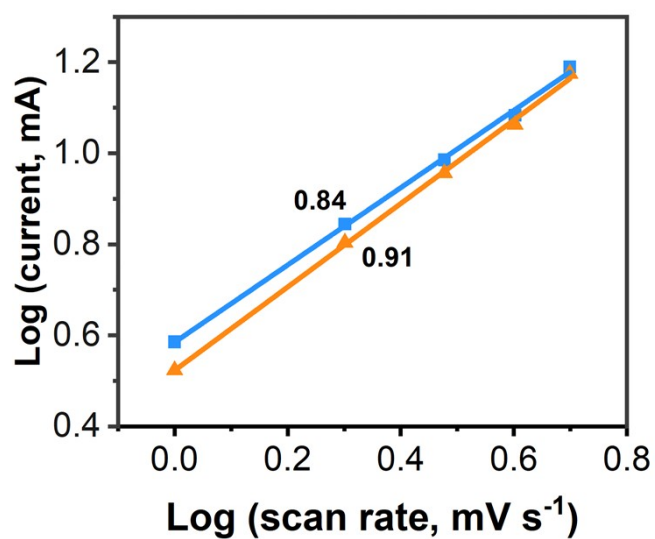


Figure S24. The linear fitting of the peak current density with different scan rates of the PZ-2OH || Ni(OH)₂ full cell.

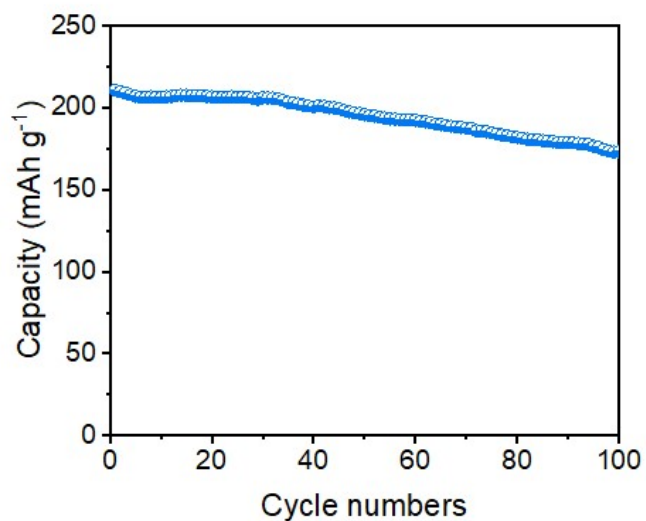


Figure 25. Cycle performance of discharge capacity at the current density of 1C.

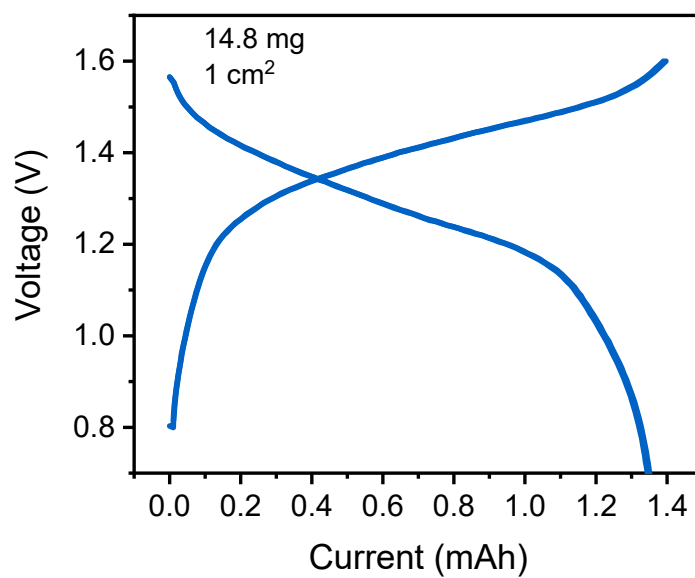


Figure S26. The discharge-charge curves of PZ-2OH || Ni(OH)₂ cell with mass-loading of 14.8 mg at the current density of 2 A cm⁻².

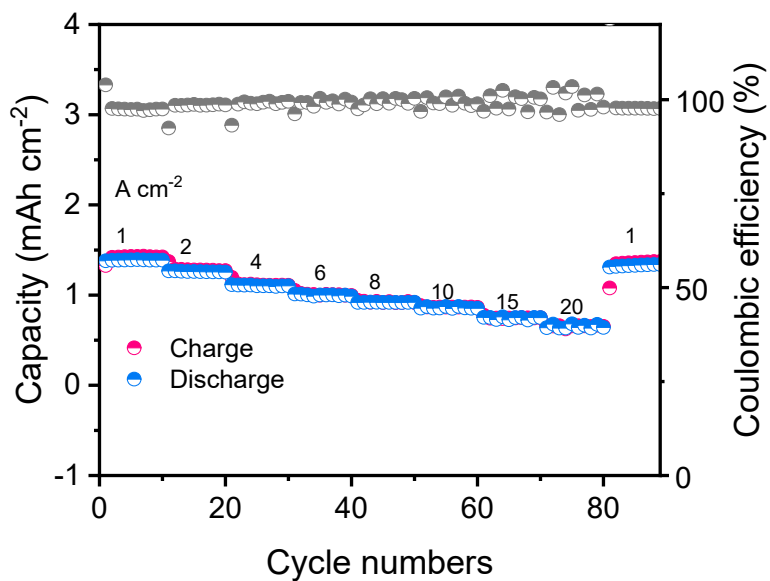


Figure S27. The rate capability of PZ-2OH || Ni(OH)₂ cell with the mass-loadings of 10 mg at different density current.

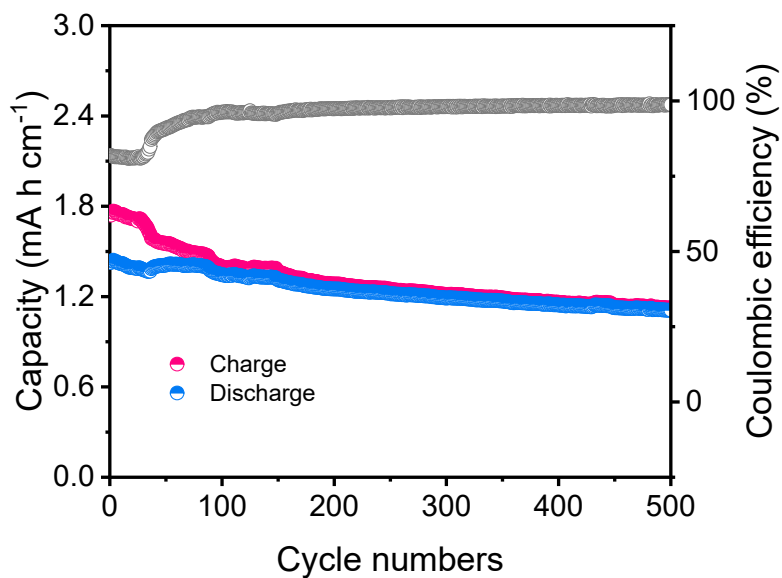


Figure 28. Cycle performance at 2 A cm⁻² with mass-loading of 10 mg.

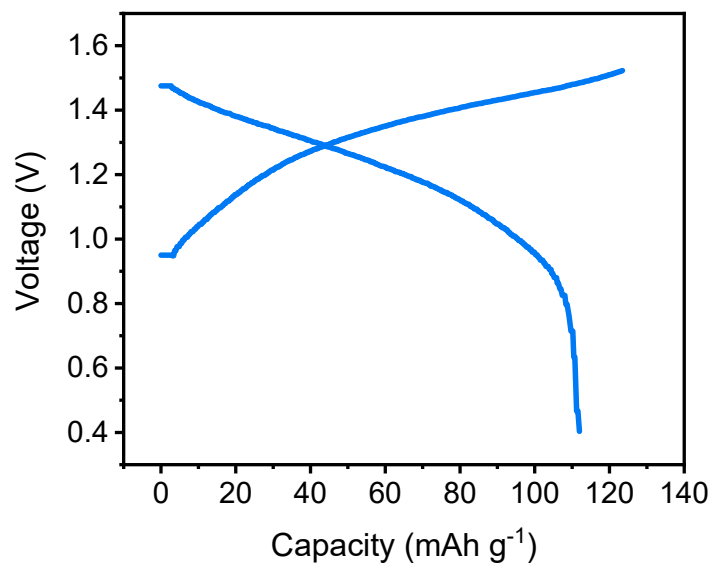


Figure 29. The discharge-charge curves of PZ-2OH || Ni(OH)₂ cell based on the n/p ratio ratio (1:1.5).

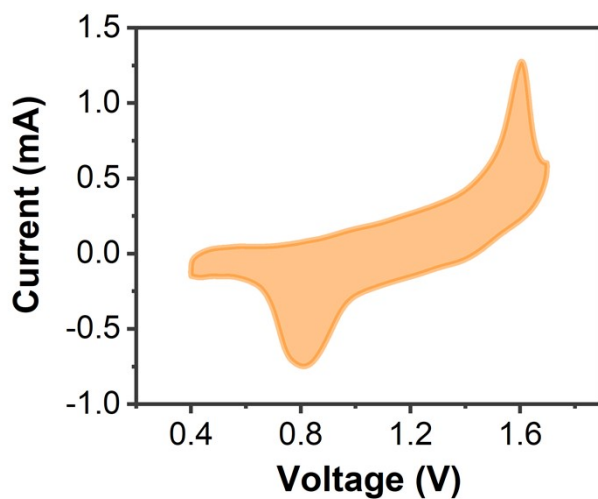


Figure S30. CV curves of PZ-2OH || Air battery at scan rate of 5 mV s⁻¹.

Table S1. The summary of the free energy of neutral and charged system and calculated electron affinity (EA).

Material	Free energy of neutral system (Hartree)	Free energy of charged system (Hartree)	EA (Hartree)	EA (kcal/mol)
PZ	-571.6190	-572.8284	-1.2094	-768.91
PZ-OH	-646.8415	-648.0456	-1.2041	-755.58
PZ-2OH	-722.0589	-723.2564	-1.1975	-751.44

Table S2. Calculated solvation energy and reduction potential of the phenazine derivatives.

Phenazine Derivative	Calculated Solvation Energy (eV)	Calculated Redox Potential (vs Hg/HgO)	Measure Redox Potential (vs Hg/HgO)
PZ	/	/	-0.78
PZ-OH	-0.39227	-0.976	-0.9
PZ-2OH	-0.43181	-0.995	-1.07
PZ-3OH	-0.47549	-1.017	/
PZ-4OH	-0.51573	-1.037	/

Table S3. Comparison of the cell discharge voltages of organic electrode material in acid electrolytes, mild electrolytes, and alkaline electrolytes.

	Electrolyte	Voltage	Ref.
PTO MnO ₂	2M MnSO ₄ +2M H ₂ SO ₄	0.9 V	6
Pb PCHL-rGO	5 M H ₂ SO ₄ electrolyte	1 V	7
All organic	Protonated pyridinium triflate derivates	0.52 V	8
Zn TABQ	1M ZnSO ₄	0.9 V	9
KFeMnHCF PTCDI	22 M KCF ₃ SO ₃	1.2 V	10
Mn 4-Cl-BQ	1M Mn(CF ₃ SO ₃) ₂	1.27 V	11
P14AQ Ni(OH) ₂	13 M KOH	0.96 V	12
PAQS Ni(OH) ₂	10 M KOH	1.12V	13
This work	6 M KOH+1M LiOH	1.4 V	

Table S4. Comparison of the comprehensive performances of commercial alkaline nickel-based batteries.

System	Price (\$/kg)	Cycle Numbers	Voltage (V)	Nontoxicity	Energy density (Wh/kg)
This work	3-10	9000	1.5	5	120
Cd Ni	12-14	500-2000	1.2	1	60
Metal Ni	40-43	500-5000	1.2	3	100
Zn Ni	2.9-3.5	300-2000	1.7	4	160

Note: The price is counted according to the anode material.

Nontoxic indicators are graded from 1 to 5, smaller non-toxic data means more toxic

Reference

1. T. Lu and F. Chen, *Journal of computational chemistry*, 2012, **33**, 580-592.
2. S. Deng, Z. Tie, F. Yue, H. Cao, M. Yao and Z. Niu, *Angewandte Chemie*, 2022.
3. C. Han, H. Li, Y. Li, J. Zhu and C. Zhi, *Nature Communications*, 2021, **12**, 1-12.
4. C. Seillan, H. Brisset and O. Siri, *Organic Letters*, 2008, **10**, 4013-4016.
5. A. Hollas, X. Wei, V. Murugesan, Z. Nie, B. Li, D. Reed, J. Liu, V. Sprenkle and W. Wang, *Nature Energy*, 2018, **3**, 508-514.
6. Z. Guo, J. Huang, X. Dong, Y. Xia, L. Yan, Z. Wang and Y. Wang, *Nature Communications*, 2020, **11**, 959.
7. F. Yue, Z. Tie, S. Deng, S. Wang, M. Yang and Z. Niu, *Angewandte Chemie International Edition*, 2021, **60**, 13882-13886.
8. R. Emanuelsson, M. Sterby, M. Strømme and M. Sjödin, *Journal of the American Chemical Society*, 2017, **139**, 4828-4834.
9. Z. Lin, H.-Y. Shi, L. Lin, X. Yang, W. Wu and X. Sun, *Nature Communications*, 2021, **12**, 4424.
10. L. Jiang, Y. Lu, C. Zhao, L. Liu, J. Zhang, Q. Zhang, X. Shen, J. Zhao, X. Yu and H. Li, *Nature Energy*, 2019, **4**, 495-503.
11. S. Bi, S. Wang, F. Yue, Z. Tie and Z. Niu, *Nature communications*, 2021, **12**, 6991.
12. Y. Li, L. Liu, C. Liu, Y. Lu, R. Shi, F. Li and J. Chen, *Chem*, 2019, **5**, 2159-2170.
13. Y. Liang, Y. Jing, S. Gheyhani, K.-Y. Lee, P. Liu, A. Facchetti and Y. Yao, *Nature materials*, 2017, **16**, 841-848.